supplementary materials

Fe/Fe_3C nanoparticles in-situ doped carbon nanofiber embedded in rGO as high-performance anode electrocatalysts of microbial fuel cells

Tingli Ren[a], Yuanfeng Liu[a], Xiaoqiu Lin[a], Congju Li[*,a]

[a] *School of Energy and Environmental Engineering, University of Science and Technology Beijing, Beijing 100083, China; Beijing Key Laboratory of Resource-oriented Treatment of Industrial pollutants, Beijing 100083, China*

Corresponding Author.
E-mail address: congjuli@126.com (Congju Li)

Table S1 The components of solution in MFCs.

Samples	Components	Purity	Source	Contents (L^{-1})
The anode solution	CH_3COONa	≥98%	Sigma-Aldrich	1 g
	NH_4Cl	≥99%	Macklin	0.1 g
	NaCl	≥99%	Hopebio	0.5 g
	$NaHCO_3$	≥99%	Sinopharm Chemical Reagent	1 g
	KH_2PO_4	≥99%	Macklin	0.53 g
	Na_2HPO_4	≥99%	Macklin	3.3 g
	Trace element			1 ml
	Vitamin solution			1 ml
The cathode solution	$K_3[Fe(CN)_6]$	≥99%	Yong Da Chemical Reagent	16.4 g
Trace element	HCl (25%)	37%	Sinopharm Chemical Reagent	10 mL
	$FeCl_3 \quad 4H_2O$	≥98%	Sigma-Aldrich	1.5 g

	$ZnCl_2$	≥99%	Sigma-Aldrich	0.07 g
	$MnCl_4 \quad 4H_2O$	≥99%	Sigma-Aldrich	0.1 g
	$CoCl_2 \quad 6H_2O$	98%	Sigma-Aldrich	0.19 g
	$CuCl_2 \quad 2H_2O$	≥99%	Sigma-Aldrich	2 mg
	$NiCl_2 \quad 6H_2O$	≥98%	Sigma-Aldrich	0.02 g
	$NaMoO_4 \quad H_2O$	≥99%	Sigma-Aldrich	0.04 g
vitamin solution	Biotin	≥98%	Sigma-Aldrich	20 mg
	Folic acid	≥98%	Sigma-Aldrich	20 mg
	pyridoxine-HCl	≥98%	Sigma-Aldrich	100 mg
	Thiamine-HCl $\quad 2H_2O$	≥99%	Sigma-Aldrich	50 mg
	rivoflavin	100%	Santa cruz	50 mg
	nicotinic acid	≥99%	Absin	50 mg
	D-Ca-pantothenate	≥98%	Sigma-Aldrich	50 mg

	vitamin B12	≥99%	Cayman chemical	50 mg
	para-aminobenzoic acid (PABA)	≥99%	Sigma-Aldrich	50 mg
	thioctic acid	≥98%	Raybiotech	50 mg
	nicotinamide	≥98%	Absin	50 mg
	lipoic acid	≥98%	Sigma-Aldrich	50 mg
	hemin	≥90%	Sigma-Aldrich	50 mg
	1,2-Nnphthoquinone	≥99%	Sigma-Aldrich	50 mg
	vitamin K2	≥98%	Cayman chemical	50 mg

1. Calculation methods:

1.1 The specific capacitance (C_p) values

The specific capacitance (mF cm^{-2}) of the electrode materials can be calculated based on the following formula,

$$C_p = \frac{1}{2Ak(V_a - V_b)} \int_{V_a}^{V_b} IdV \quad (1)$$

Where I was the real-time current, mA; V_a, V_b and V represented the initial potential (V), the final potential (V) and the real-time potential (V), respectively; A represented the anode surface area (4 cm^{-2}); k represented the scan rate of the CV curve, 0.01 V s^{-1} [1, 2].

1.2 The chemical oxygen demand (COD) removal efficiency

The removal efficiency of chemical oxygen demand (mg L^{-1}) was measured according to the digestion method [3].

$$COD(\%) = \frac{(COD_{in} - COD_{out})}{COD_{in}} \times 100\% \quad (2)$$

Where COD_{in} *and* COD_{out} represented the inlet COD content and outlet COD content (mg L^{-1}), respectively.

1.3 Coulombic efficiency (CE, %)

CE (%) was calculated based on the following formula,

$$CE = \frac{8 \int_0^t Idt}{FV\Delta COD} \quad (3)$$

Where I was the real-time current, A; F represented Faraday constant, 96500 C

mol^{-1}; V represented the volume of the anode chamber, 0.118 L; ΔCOD refered to the difference between influent and effluent, mg L^{-1}.

1.4 The polarization curve and power density

The polarization curve (J, mA m^{-2}) and power density (P, mW m^{-2}) were calculated based on LSV of MFCs, and the calculation formula is as follows.

$$P=(U\times I)/A,\ J=I/A \tag{4}$$

Where U was the cell voltage (V); R was the external resistance (Ω), I was current (A); A was electrode area (80% of the electrode area, m^{-2}).

2. Experimental section

2.1 Preparation of NCNFs@Fe/Fe_3C and NCNFs

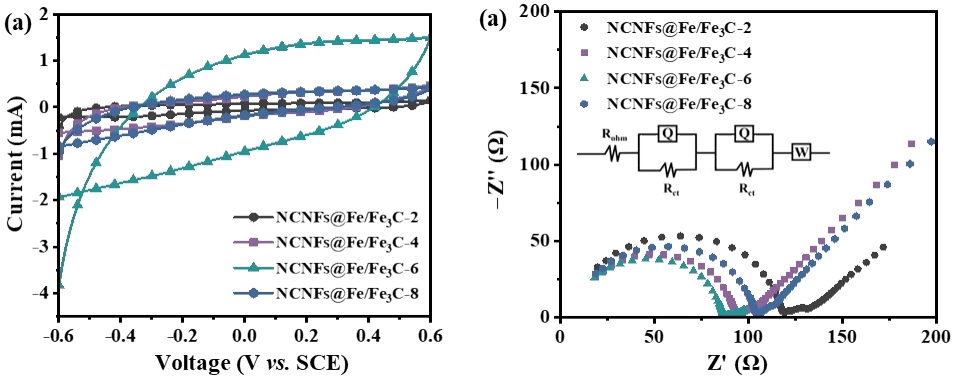

Fig. S1. (a) CV curves, (b) Nyquist curves of NCNFs@Fe/Fe_3C-x (x=2, 4, 6, 8).

As shown in Fig. S1a, the CV curve of NCNFs@Fe/Fe_3C-6 had the largest redox loop area and the highest capacitive current response, which meant that it had the best capacitive performance compared with other samples. The ohmic resistance (R_{ohm}) and charge transfer resistance (R_{ct}) of different anodes were obtained using the fitted equivalent circuit in the inset of Fig. S1b. They exhibited similar R_{ohm} (8.592-9.243 Ω) while exhibiting significantly different R_{ct}. The R_{ct} of NCNFs@Fe/Fe_3C-6 was 76.58 Ω, which was lower than that of NCNFs@Fe/Fe_3C-2 (108.20 Ω), NCNFs@Fe/Fe_3C-4 (83.02 Ω), NCNFs@Fe/Fe_3C-8 (93.22 Ω).

With the improving of Fe/Fe_3C concentration, the electrochemical property first rose and then declined. The NCNFs@Fe/Fe_3C-6 reached the maximum redox peak current and the smallest resistance. It means that the charge transfer rate of NCNFs@Fe/Fe_3C-6 was the fastest, which was determined by its rough and unique surface. Comparing the electrochemical properties of NCNFs@Fe/Fe_3C-x (x=2, 4, 6, 8), the NCNFs@Fe/Fe_3C-6 with a relatively large capacitance and excellent

conductivity (Fig. S1), was chosen for the in-depth study, abbreviated as NCNFs@Fe/Fe_3C.

2.2 Anode biofilms characterization

Before SEM characterization, 5 wt% glutaraldehyde (Grade II, 25% in H_2O, Sigma-Aldrich) solutions were dropped on the anode samples, chemically dehydrated with gradient contents of ethanol aqueous solutions (30–70 vol%) and dried in an oven at 40 °C for 2 h to maintain the original structures of bacterial cells.

The survival state of the bacterial cells on different anodes was observed by confocal scanning laser microscopy (CLSM, LSM800, ZEISS, Germany). For CLSM imaging, a calcein-AM/PI double staining kit composed of green fluorescent calcein AM and red fluorescent calcein PI was used to distinguish the living/dead bacterial cells.

3 Results and discussion

3.1 Characterization of the anode materials

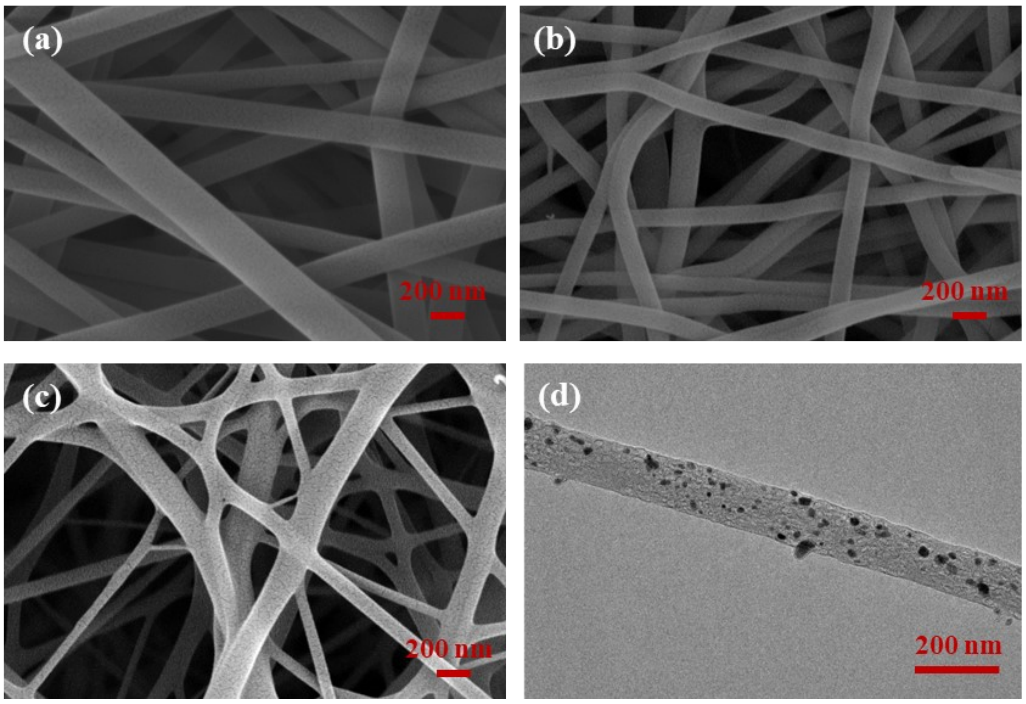

Fig. S2. SEM images of (a) nanofibers (NFs); (b) iron-doped nanofibers (Fe-NFs); (c) the diameter of nitrogen-doped carbon nanofibers (NCNFs); (d) TEM image of NCNFs@Fe/Fe_3C.

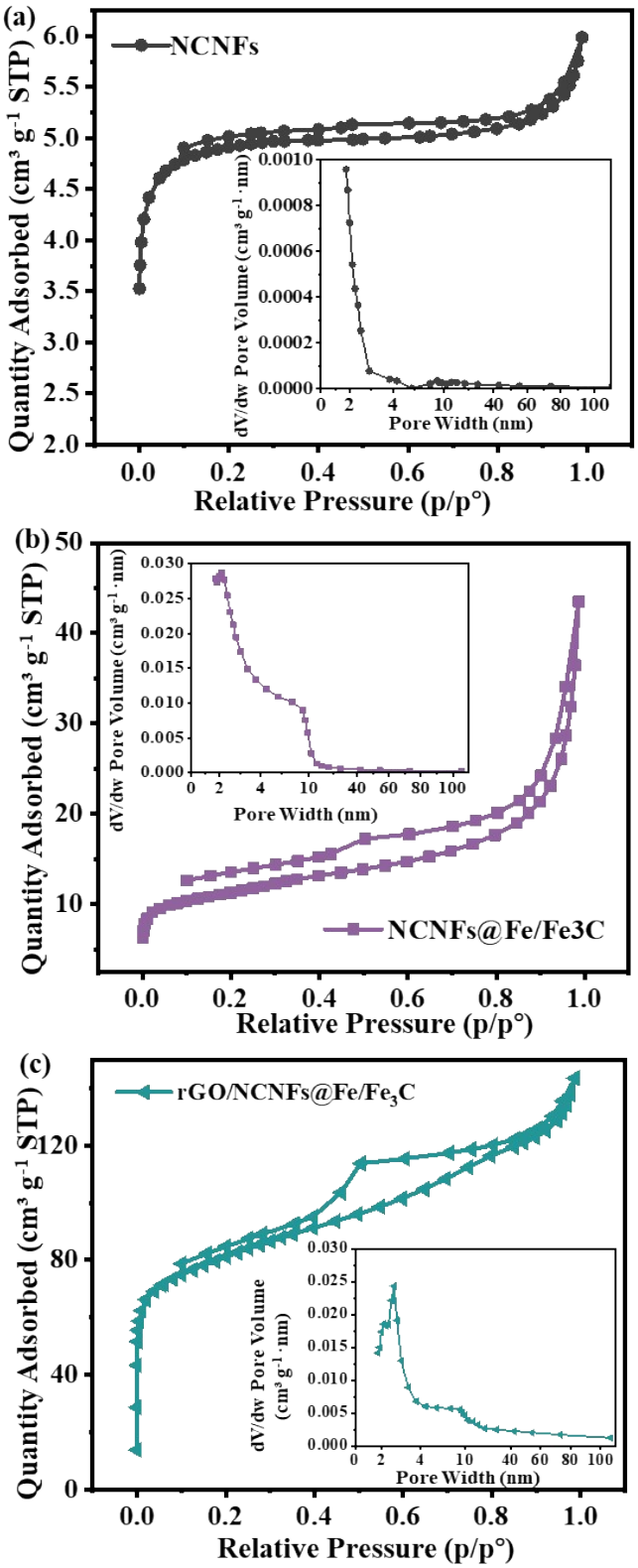

Fig. S3. Nitrogen adsorption–desorption isotherms and corresponding pore size distributions of (a) NCNFs; (b) NCNFs@Fe/Fe_3C and (c) rGO/NCNFs@Fe/Fe_3C.

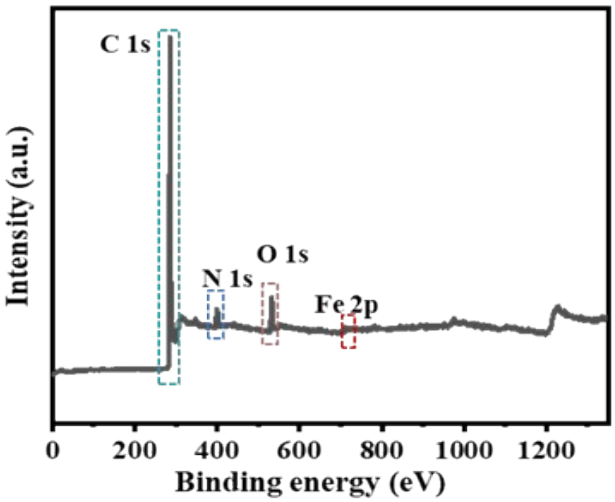

Fig. S4. The full XPS spectra

3.2. Electrochemical analysis

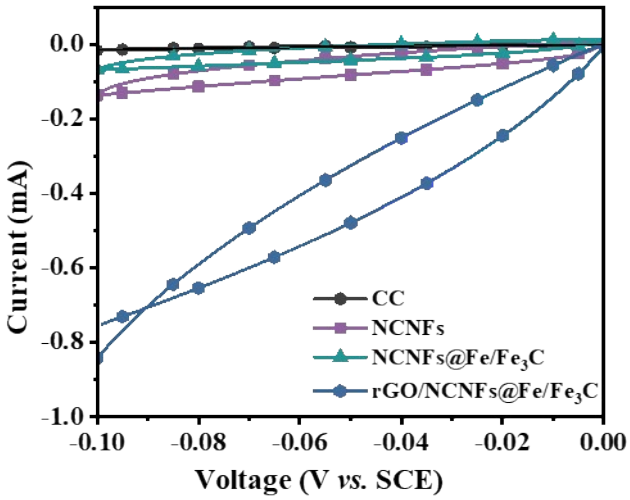

Fig. S5. CV curves of different anodes.

The CV curves of different anodes between -0.1 V and 0 V (with a scan speed of 0.01 V s^{-1}) were measured using an electrochemical workstation with a conventional three-electrode system, as shown in Fig. S5. The prepared anodes with electrocatalysts were regarded as the working electrodes, while the graphite and saturated calomel electrode (SCE) were used as the counter and reference electrodes, respectively. Additionally, the anode solution was used as the electrolyte solution. The specific capacitance was calculated by Origin software.

Table S2. The fitted values of R_{ohm} and R_{ct} of different anodes.

Samples	**R_{ohm}**	**R_{ct}**
CC	6.76	72.78
NCNFs	6.45	62.12
NCNFs@Fe/Fe_3C	7.09	58.68
rGO/NCNFs@Fe/Fe_3C	7.20	57.22

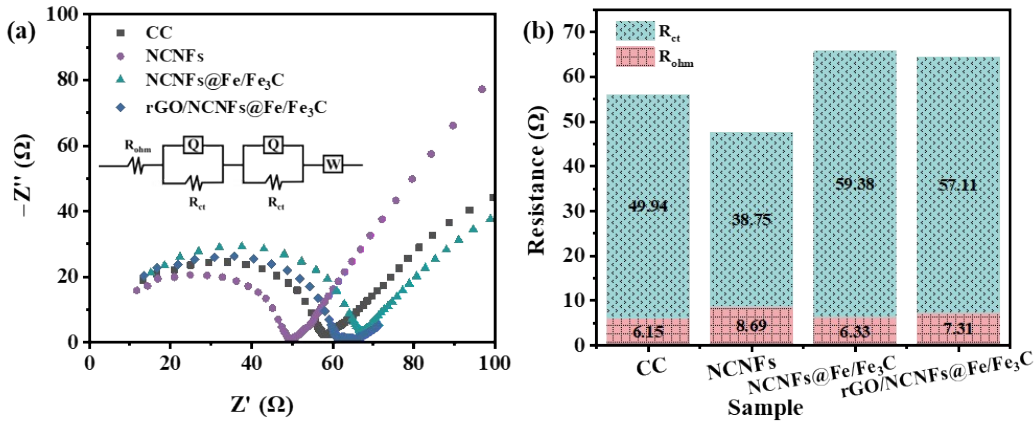

Fig. S6. (a) Nyquist curves, and (b) the fitted values of R_{ohm} and $_{Rct}$ obtained at the open circuit potential with Fe(CN) $6^{3-/4-}$ (1 mM each) in anode solution.

3.3. MFC performance

The CV curves in Fig. 3d were measured based on MFC devices with a conventional three-electrode system. The anode and cathode of the MFCs were regarded as the working and counter electrodes, respectively, while the saturated calomel electrode (SCE) was regarded as the reference electrode , and the electrode solution for the measurement was the anode solution.

3.4. Biofilm morphology and structure

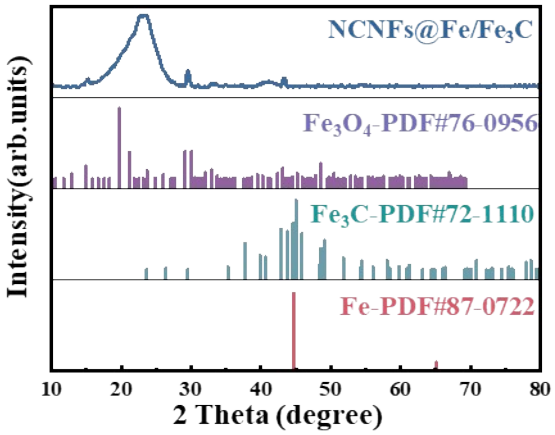

Fig. S7. The XRD image of the biofilm of the NCNFs@Fe/Fe_3C anode

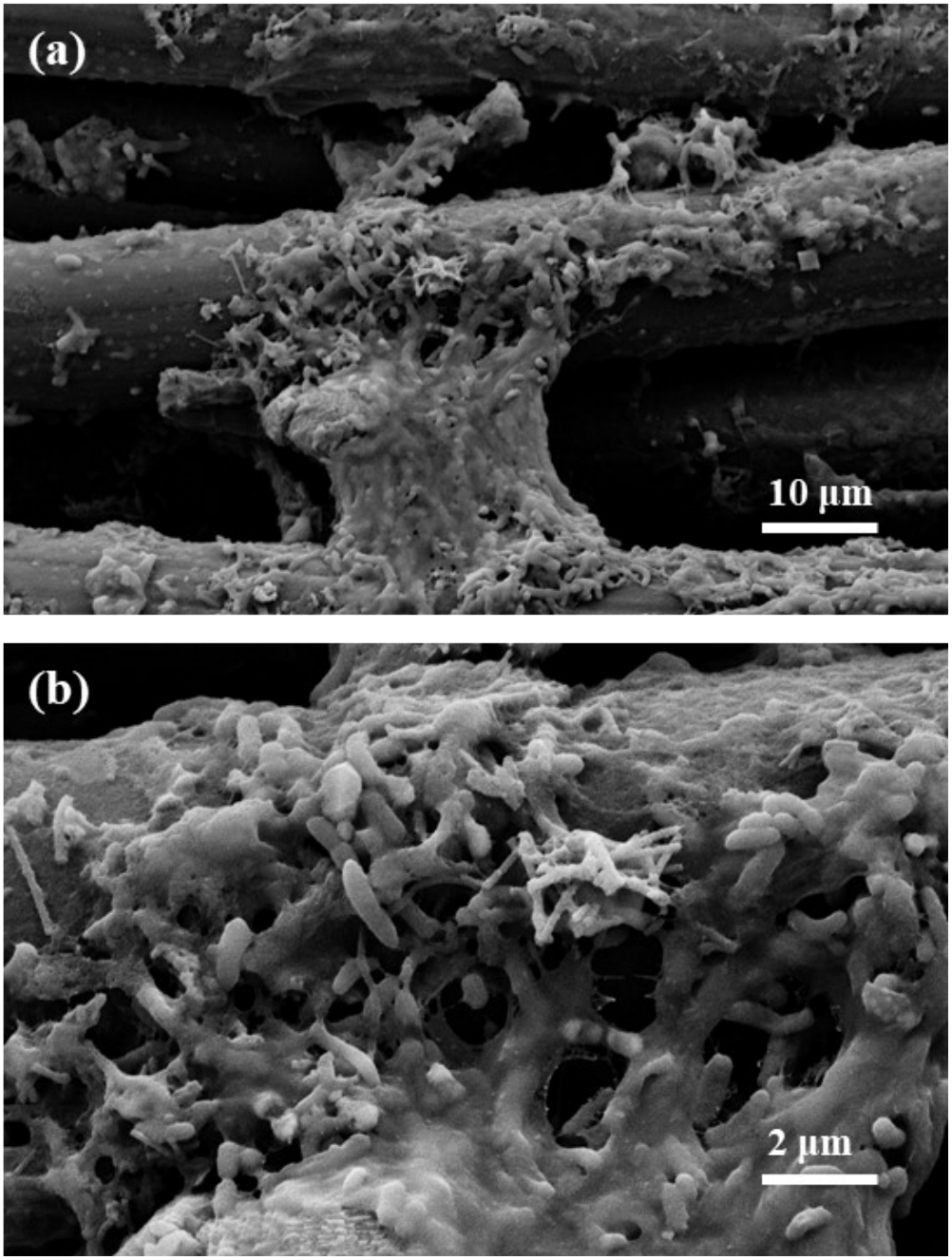

Fig. S8. SEM images of rGO/NCNFs@Fe/Fe_3C.

The aerogel structure of rGO/NCNFs@Fe/Fe_3C provided sufficient pores increasing the specific surface area of the anode. Bacteria could attach to the pores, resulting in an elevated microbial loading of the anode, which facilitated the formation of a continuous dense biofilm.

Table S3. Diversity and abundance index of the microbial community on different anodes.

Samples	Shannon[a]	Simpson[b]	Coverage	ACE[c]	OTUs
CC	1.655	0.262	1	18.000	237
NCNFs	1.678	0.212	0.999	19.458	262
NCNFs@Fe/Fe_3C	1.522	0.234	1	20.000	285
rGO/NCNFs@Fe/Fe_3C	1.492	0.309	1	22.000	323

a. The diversity index of the microbial community. A higher value indicates more diversity.

b. The evenness index of the microbial community. A higher value indicates more evenness.

c. The abundance index of the microbial community. A higher value indicates more abundance.

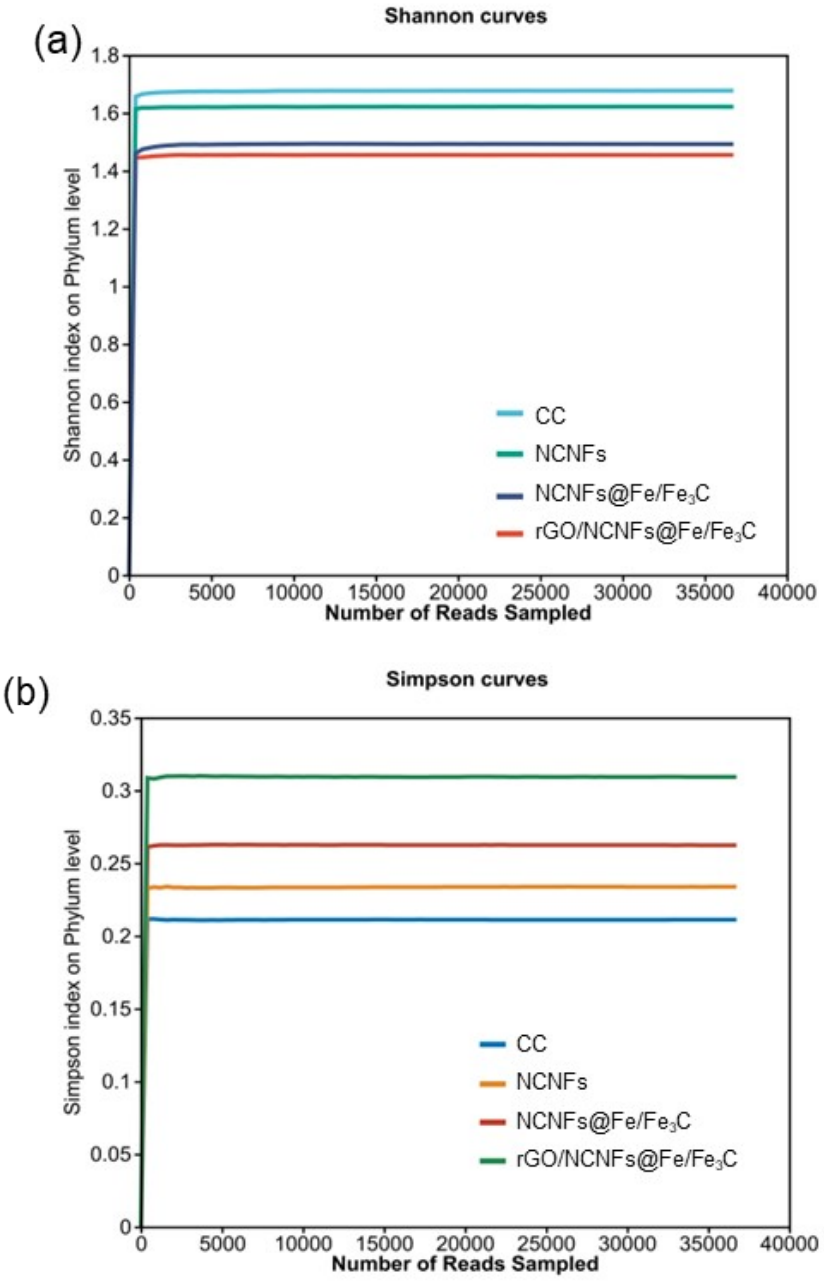

Fig. S9. Rarefaction curves of (a) Shannon and (b) Simpson.

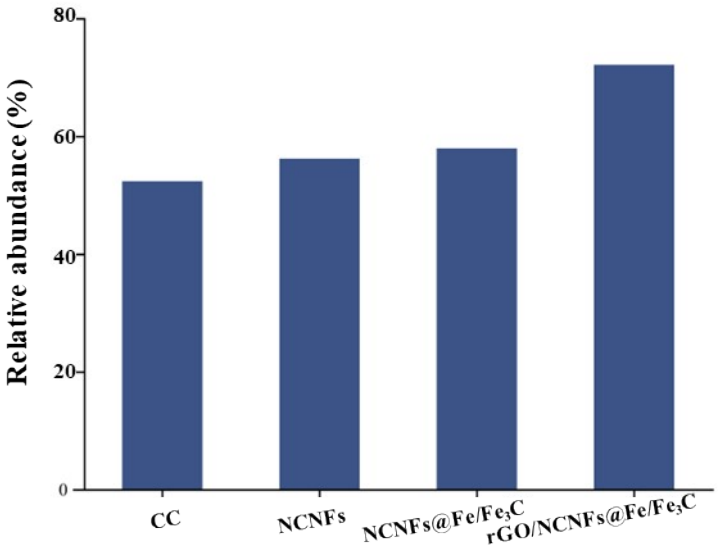

Fig. S10. The relative abundance of electroactive microbial communities of different anode samples at the phylum level

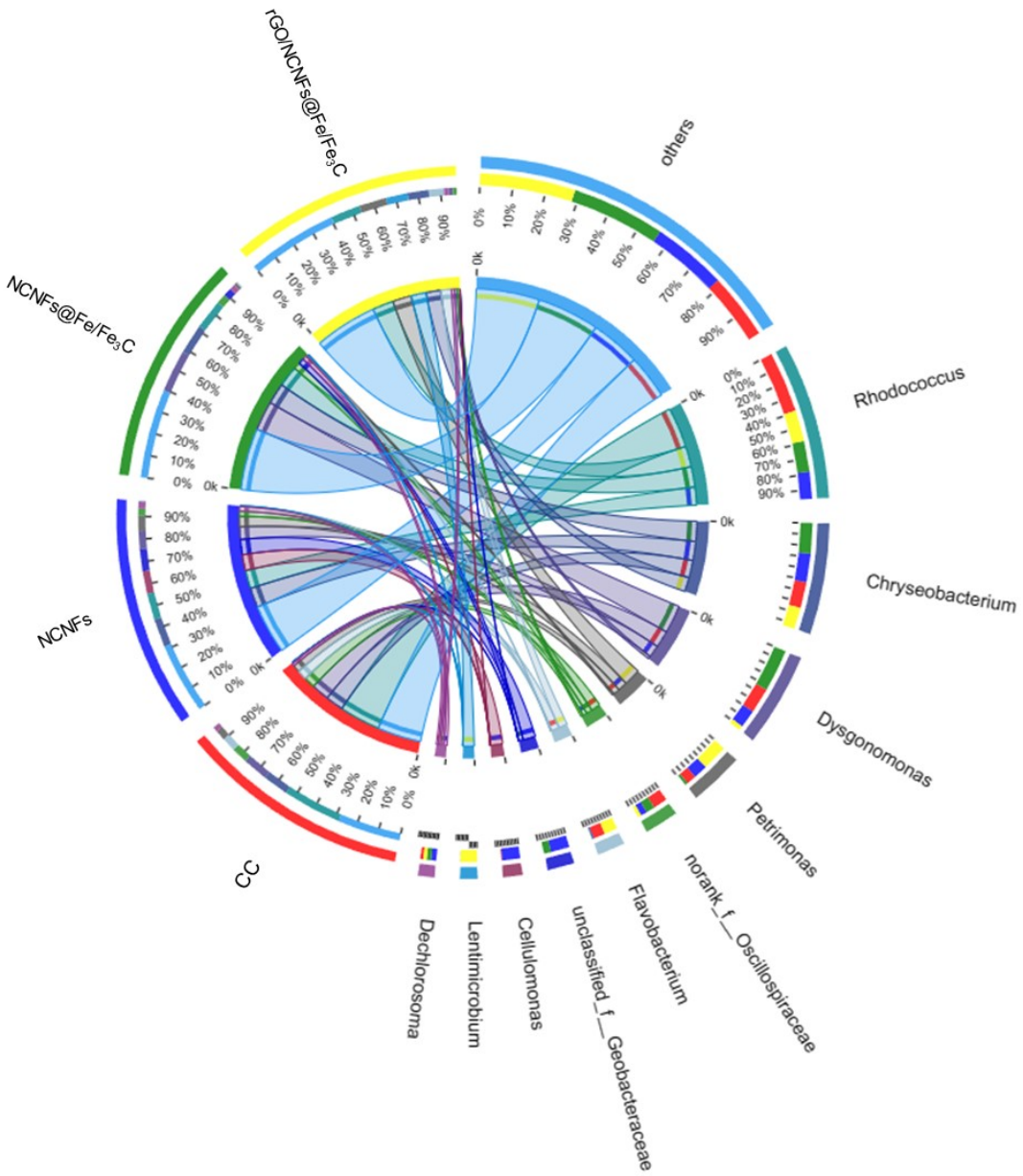

Fig. S11. Microbial community structure of different anode samples at the genus level

References

1. T. Deng, X. Y. Shi, W. Zhang, Z. Z. Wang and W. T. Zheng, *Nanotechnology*, 2021, **32**, 7.
2. J. B. Tang, W. X. Huang, X. Lv and Q. W. Shi, *Nanotechnology*, 2021, **32**, 9.
3. C. Wei, H. P. Wu, Q. P. Kong, J. Y. Wei, C. H. Feng, G. L. Qiu, C. H. Wei and F. S. Li, *Journal of Environmental Management*, 2019, **246**, 324-333.